Title
Ideal spatio-temporal pulse distribution for exawatt-scale lasers based on simultaneous chirped beam and chirped pulse amplification.

Journal
Optics Express, 31(4)

ISSN
1094-4087

Authors
Chesnut, KD
Barty, CPJ

Publication Date
2023-02-13

DOI
10.1364/oe.480302

Research Article Vol. 31, No. 4 / 13 Feb 2023 / Optics Express 5687
Optics EXPRESS

Ideal spatio-temporal pulse distribution for exawatt-scale lasers based on simultaneous chirped beam and chirped pulse amplification

K. D. CHESNUT* AND C. P. J. BARTY

Department of Physics & Astronomy, University of California – Irvine, Irvine, CA 92782, USA
*kyle.chesnut@uci.edu

Abstract: This paper presents the ideal spatio-temporal pulse structure that is required to produce exawatt-scale pulses based on simultaneous chirped beam and chirped pulse amplification in a Nd:Mixed-glass laser system. It is shown, that a 100 fs Fourier transform-limited pulse is created from a 20 ns duration stretched beam-pulse after propagating through an appropriate six-grating compressor arrangement. Quantitative results, from a ray-tracing model of the six-grating compressor, provide the detailed spatio-spectral and spatio-temporal pulse distributions of the stretched pulse along with the higher-order phase distortions compensated by this pulse compression scheme.

1. Introduction

High-intensity laser systems have grown tremendously over the past few decades based on chirped pulse amplification (CPA) technology [1]. Here, intensity induced damage to the amplifier medium is mitigated by stretching the optical pulse in time prior to amplification [2]. Most recent efforts at ELI-NP have pushed high-intensity lasers based on CPA in Ti:Sapphire to 10 PW peak-power, ~243 J in ~22.7 fs, from a single beam line [3]. Extension of Ti:Sapphire systems to higher powers is limited by available crystal sizes and, more importantly, by final optics issues. In all CPA systems the intensity is highest on the final grating of the pulse compressor and all down-stream optics. Overcoming field-induced damage on these optics is a primary challenge with respect to extending visible and IR laser systems to the exawatt-class peak powers. At intensities above 10^{13} W/cm^2, the laser field strength is sufficient to liberate bound electrons from dielectric and metal surfaces. At these levels, damage is determined not by the quality of the optical coating but by the intrinsic limit of valence electron ionization. Assuming an ultimate final optic intensity limit of 100 mJ/cm^2 at 10 fs, implies a final optics area of at least 10 m^2 for exawatt pulse production. The upstream gratings within a four-grating compressor require an even larger area. Three strategies have been proposed to circumvent this issue, namely:

(a) Coherently combine multiple independent 10 PW, CPA beamlines—such as the Ti:Sapphire system mentioned above—with an array of focusing optics post-compression [4]. With this technique each amplifier can have a different prompt wavefront distortion shot-to-shot making phasing a challenge and lowering the final achieved focused intensity. This issue becomes more prominent as the compressed pulse duration from the independent amplifiers is decreased.

(b) Compress a single large-area, high-energy beamline via a tiled-grating compressors and final optics [5,6]. Large-aperture (40 cm x 40 cm) Nd:Mixed-glass lasers have demonstrated kJ-level energy with ~100 fs pulse durations [7,8]. The potential exists to extract up to ~25 kJ given a ~20 ns stretched pulse [9]. Additionally, a wide-angle noncollinear optical parametric CPA system (WNOPCPA) has been proposed to produce ~7 fs pulses with energies exceeding 500 J to reach exawatt peak-power [10]. Both amplification schemes

#480302 https://doi.org/10.1364/OE.480302
Journal © 2023 Received 10 Nov 2022; revised 4 Jan 2023; accepted 18 Jan 2023; published 1 Feb 2023

Optics EXPRESS

would require beam expansion to reduce the fluence below the damage threshold of the final optics along with a grating compressor comprised of many coherently tiled, meter-scale gratings. Each of these gratings has five degrees-of-freedom that need to be aligned with accuracy on the order of ~1 μRad about the rotation axes and ~10 nm along the translation axes to reach an acceptable level of wavefront quality and pulse compression [11].

(c) The pulse spectral content is chirped both in time and space as it transits the amplifier—a technique which we will call chirped pulse juxtaposed with beam amplification (CPJBA) for brevity [12,13]. The CPJBA approach produces a ~20 ns stretched pulse that can safely extract up to 25 kJ from a single, large-area Nd:Mixed-glass amplifier and be recompressed down to a Fourier transform limit (FTL) pulse of ~100 fs without the need for tiled gratings. To avoid damage on the final optic the pulse is split into multiple identical copies by a dispersion balanced beam splitter arrangement prior to complete compression by final grating pairs. The fundamental advantages of this approach are compatibility with existing, high-efficiency, high-damage threshold grating designs, use of monolithic, non-tiled gratings in the compressor, amplification in a single amplifier aperture allowing for a singular wavefront distortion and the phasing of inherently similar beamlets.

This paper covers the compression scheme of CPJBA, patented in 2004 and first presented at the International Committee on Ultra-High Intensity Lasers Conference 2014, which was proposed as an analog technique to go beyond the stretched pulse limits of CPA [12,13]. The two laser architectures, based on direct amplification, that have been constructed to produce multi-petawatt peak-power are kJ-class amplifiers based on Nd:Mixed-glass [8] and fs-class amplifiers based on Ti:Sapphire [3,14]. A third laser architecture, based on optical parametric chirped pulse amplification (OPCPA), has achieved a 4.9 PW peak-power pulse at the CAEP-PW laser [15] along with several planned multi-petawatt peak-power facilities awaiting commissioning [16]. Scaling high-intensity lasers towards the exawatt class peak-power regime is largely hampered by B-integral effects (a measure of nonlinear phase accumulation due to pulse intensity) in the amplifier medium for kJ-class amplifiers and intensity dependent damage to the final compressor grating and optics for all amplifier architectures. At large B-integral values, there is risk of runaway small-scale self-focusing leading to catastrophic damage of the amplifier medium [17]. Increasing the stretched pulse duration lowers the pulse intensity and increases the amount of energy that can be safely extracted from a given amplifier. Large saturation fluence materials—such as Nd:Glass and Yb:Glass—require a larger stretched pulse duration (multi-ns) than that needed for Ti:Sapphire systems. In the case of high-energy Nd:Glass systems the B-integral limit is often based on a phenomenological operating limit of 3 with 5-6 as the upper limit [18,19]. A single NIF beamline has demonstrated 26 kJ using a 23 ns pulse for extraction [9], corresponding to an operating fluence that is ~4 times greater than the saturation fluence of Nd:LG-770.

In CPA pulses are stretched or compressed by causing a frequency dependent group delay in the pulse, called group delay dispersion (GDD). Most commonly, stretchers generate positive GDD, where blue travels a longer distance than red, and compressors generate negative GDD, where red travels a longer distance than blue. In a grating pair compressor, the first grating induces angular dispersion on the pulse, having the red components diffract at a larger angle than the blue, and the second grating removes the angular dispersion. The path length difference of the frequency components as they travel between the two gratings produces negative GDD on the pulse. Increasing the difference in group delay between the red and blue components, to recompress a longer stretched pulse, requires that the grating pair separation is increased. This necessarily creates a larger projected area on the second grating. A standard four-grating compressor scheme for CPA would require an impractically large grating aperture to compress a ~20 ns pulse down to a ~100 fs FTL pulse. Instead, simultaneously chirping the pulse in both time and space enables a more efficient use of a fixed grating aperture for pulse compression if a novel

Optics EXPRESS

six-grating, versus a four-grating, compressor arrangement is used. We will consider the case that corresponds to an existing efficient, high-damage threshold grating design [20] and a NIF-like aperture [9], also used at high-energy laser facilities such as Omega EP [21], Laser Mega-Joule (LMJ) [22], and the Laser for Fast Ignition Experiment (LFEX) [23]. While this aperture is assumed, the following argument applies to lasers with smaller or larger apertures as well. The following presents the ideal spatio-temporal pulse structure that can be compressed to the FTL by the six-grating CPJBA compressor, as well as the higher-order phase distortions present in the stretched beam-pulse. CPJBA provides a path to extract the full 25 kJ from a NIF-like beamline and recompress the pulse to ~100 fs—breaking through the current limits of high-intensity laser technology to potentially produce a 0.2 exawatt peak-power pulse post-compression.

2. Chirped pulse juxtaposed with beam amplification (CPJBA)

In CPA a laser pulse is temporally stretched to reduce the pulse intensity in the amplifier medium. Post amplification, the temporally chirped pulse is compressed with two grating pairs in a traditional four-grating compressor arrangement that induce a negative GDD on the pulse, which is linearly proportional to the normal separation of the two gratings that compose the grating pair [24]. The amount of GDD that can be removed by a grating pair is limited, in part, by the maximum available grating aperture. The tooling used by Plymouth Grating Laboratory and Lawrence Livermore National Lab to produce multi-layer dielectric (MLD) gratings can be extended to produce 2 m aperture gratings with further process development [25]. In this paper we presume the availability of 2 m wide by 40 cm tall gratings; however, the argument that follows is valid for any fixed maximum grating aperture size. For large beams, the CPA scheme effectively utilizes only a small fraction of the grating aperture for temporal pulse compression. As illustrated in Fig. 1 below, the grating aperture size, along with the spatial and spectral width of the temporally chirped pulse, are the limiting factors in the maximum normal separation distance between two gratings of a grating pair. The maximum normal separation is given by,

$$L_{max} = \frac{G - \frac{w}{\cos(\gamma)}}{\tan(\theta_r) - \tan(\theta_b)}, \tag{1}$$

where G is the width of the second grating, w is the input beam width, γ is the input angle to the first grating, and θ_b and θ_r are the diffracted angles of representative blue and red portions of the pulse spectrum respectively. In addition to the intensity dependent final optic damage, a main challenge in achieving an exawatt-class laser is the necessity to create sufficient stretched pulse duration such that saturation may be achieved in the amplifier medium without exceeding a threshold value of nonlinear phase accumulation, i.e. B-integral. In the NIF ARC PW laser beam line, the stretched pulse duration is ~1.2 ns. At this duration approximately 1 kJ may be extracted safely in a 18.5 cm by 37 cm beamlet [26]. To extract the full 25 kJ of stored energy from a 37 cm by 37 cm NIF-like amplifier and maintain a B-integral of < 5, the pulse must be stretched to >20 ns. For exawatt-class peak-power production, and to utilize the full bandwidth of a Nd:Mixed-glass amplifier, this 20 ns stretched pulse must be compressed to ~100 fs. Given a maximum grating aperture of 2 m with a high-damage threshold grating design [20], this compression ratio requires a grating aperture width of 6.14 m in the plane of diffraction for the second and third grating. With an optimistic damage fluence threshold of 1 J/cm^2, the height of the gratings must be 5.4 m for the total area of the final grating aperture to sufficiently reduce the beam fluence. The end result, assuming the maximum grating size posited above, necessitates the tiling of 11 grating apertures for gratings 1 and 4, and the tiling of 44 grating apertures for gratings 2 and 3 for a total of 110 gratings and a total grating area of 835,920 cm^2.

By simultaneously spatially and temporally chirping the spectral content of the pulse, one can better utilize the temporal compressive effect of a grating pair with a fixed grating aperture.

Optics EXPRESS

Spatial chirp, as it is commonly defined, is a spatio-temporal distortion that results in the different frequency components of a pulse spatially separated transverse to the direction of propagation [27]. Here, each frequency can be thought of as its own beamlet whose center is determined by the degree of spatial chirp, which yields a function, $x_0(\omega)$, whose derivative with respect to frequency is called the spatial dispersion. With the correct direction of input spatial chirp, the red beamlet and blue beamlet will undergo an image inversion as they travel from the first to the second grating, shown in Fig. 1(c). This enables a larger grating separation for a fixed size of the second grating with a maximum grating separation of,

$$L_{max} = \frac{G - \frac{w(2-\chi)}{\cos(\gamma)}}{\tan(\theta_r) - \tan(\theta_b)}. \tag{2}$$

To normalize the spatial chirp to the beamlet size we introduce the spatial chirp parameter χ that characterizes the total beam width expansion factor. A χ of two represents a spatial chip resulting in a beam width twice the original width (i.e. the centers of the red beamlet and blue beamlet are separated by the original beam width, $x_0(\omega_r) - x_0(\omega_b) = w$). For this spatial chirp the maximum separation of the grating pair is not limited by the input beam width but only by the size of the second grating aperture and the spectral bandwidth of the pulse. This allows for larger negative GDD to be generated by the grating pair for a fixed second grating aperture. For example, we consider grating pair with maximum aperture of 2 m, a groove density of 1780 lines per mm, and an input beam at an angle-of-incidence (AOI) of 76.5 degrees. With a blue wavelength of 1040 nm and red wavelength of 1080 nm, a 37 cm wide non-spatially chirped beam will generate a GDD of -3.49e7 fs^2 in this grating pair. Meanwhile, a 18.5 cm beam that is spatially chirped with a χ of two (i.e. a total beam width of 37 cm) can generate -1.83E8 fs^2 in the same grating pair—a 425% increase in GDD removed for a single grating pair.

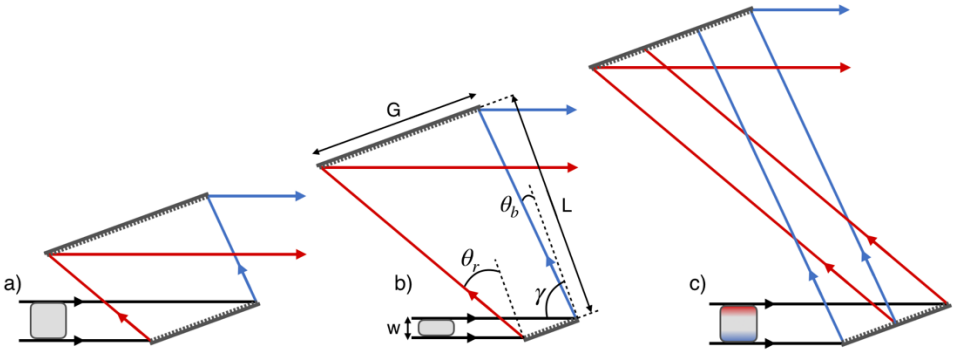

Fig. 1. Diagrams showing the maximum grating pair separation for a fixed grating aperture for a) a full-width pulse without spatial chirp b) a half-width pulse without spatial chirp and c) a spatially chirped pulse with a χ of two and full-width composed of half-width beamlets.

3. Six-grating compressor

In the compression scheme for CPJBA, shown in Fig. 2, the pulse will first travel through a standard four-grating compressor, albeit with a larger grating pair spacing, emerging partially compressed temporally but with the same degree of spatial chirp. It then enters a final grating pair, with a smaller grating separation, that removes the spatial chirp and performs a small (~15%) amount of final temporal compression.

Multi-layer dielectric gratings have been developed with a proven groove design at LLNL for the National Ignition Facility's Advanced Radiographic Capability PW laser [20] to have

Optics EXPRESS

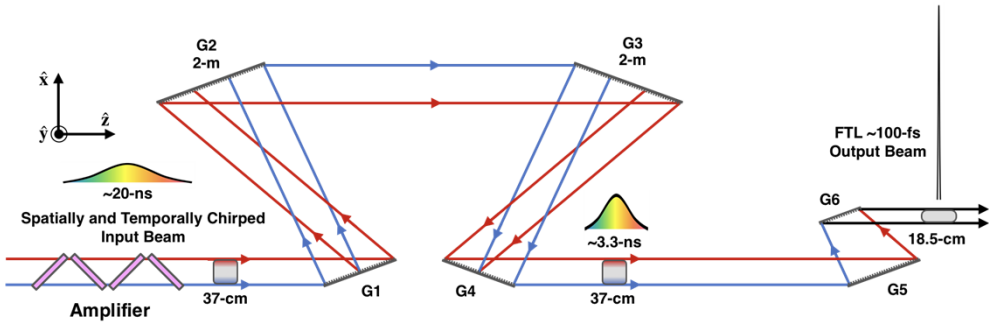

Fig. 2. Schematic of the six-grating compressor for CPJBA designed to compress a 37×37 cm aperture simultaneously spatially and temporally chirped 20 ns pulse down to an 18.5×37 cm aperture 100 fs Fourier transform-limited pulse.

meter-scale size and high-damage-threshold. These gratings are designed to be efficient at 1053 nm with a groove density of 1780 lines per mm and an AOI of 76.5 degrees [28]. Given a beam aperture from a NIF-like amplifier of 37 cm x 37 cm and an AOI of 76.5 degrees gratings G1 and G4 need to be 1.6 m wide. The modeled beam is an 8^{th}-order super-Gaussian spatial distribution with a 37 cm diameter at 1% peak fluence. This is consistent with the main laser beam in NIF that has a 37.2 cm diameter at 0.1% peak fluence [29]. The spectral pulse, shown below in Fig. 3, is also an 8^{th}-order super-Gaussian centered at 1060 nm with a FWHM of 30.2 nm, producing a sinc^2-like temporal pulse with a Fourier transform-limited FWHM of 100 fs. The red-most and blue-most spectral components are defined by the spectral components that constitute 1% of the peak spectral power. Cutting off the spectral distribution at these points has minimal effect on the temporal pulse distribution. Studies have shown that a pre-amplifier composed of Nd:phosphate glass (APG-1) mixed with Nd:silicate glass (K-824) can support this spectral bandwidth to an amplifier with total gain 10^4 and producing ~100 fs pulses [7].

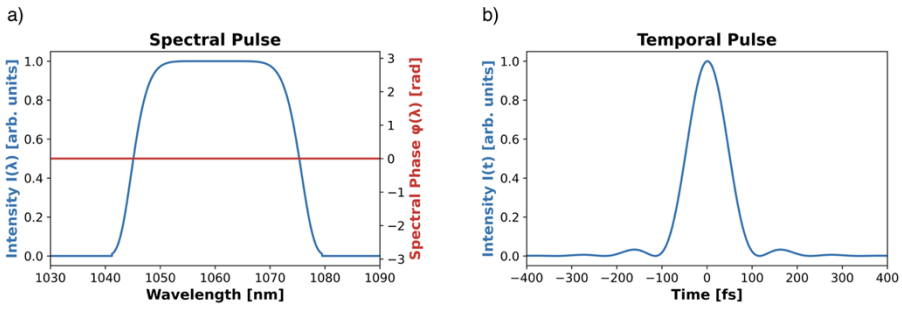

Fig. 3. Output of the CPJBA six-grating compressor. a) 8^{th}-order super-Gaussian spectral distribution of the pulse centered at 1060 nm with a FWHM of 30.2 nm and b) the Fourier transform-limited temporal pulse of the spectral distribution with a FWHM of 100 fs.

With a maximum producible grating width of 2 m, grating pairs G1-G2 and G3-G4 can have a maximum separation, along the direction normal to the grating faces, of ~1.914 m while not clipping any spectral content. The output beam from the six-grating compressor has a width of 18.5 cm in the direction of grating dispersion giving the final grating G6 width of 0.8 m. For full containment of the spectrum this allows for a maximum separation between G5 and G6 of ~0.780 m in the direction normal to the grating faces. The full geometry is summarized below in Table 1. In this six-grating compressor set-up there is a total grating separation of 4.608 m. This same

Optics EXPRESS

grating design in a standard CPA scheme is not able to handle the spectral bandwidth required for a 100 fs pulse. As shown in Eq. (1), as the spectral bandwidth increases the maximum allowable grating separation decreases; for a pulse with the spectral and spatial properties outlined above, the grating separation of G1-G2 is small enough that the second grating will physically clip the incoming beam in a standard CPA arrangement.

Table 1. Geometry of the six-grating compressor

	Dimensions		Grating Separation	
Grating	X Aperture [m]	Y Aperture [m]	Normal [m]	Transverse [m]
G1	1.6	0.4	-	-
G2	2.0	0.4	1.914	4.665
G3	2.0	0.4	-	-
G4	1.6	0.4	1.914	4.665
G5	1.6	0.4	-	-
G6	0.8	0.4	0.780	1.902

The arrangement shown in Fig. 2 still does not address the intensity damage problem on the final grating. To drop the fluence below the damage threshold of the gratings the pulse is split into 30 identical copies before entering the final grating pair. Correctly phasing together the 30 beams requires a beam splitter arrangement, shown below in Fig. 4., that imparts an equivalent amount of dispersion to each pulse copy by having each beamlet experience the same number of transmission events [13]. After the final grating pairs, the identical beamlets are coherently combined using a tiled, parabolic mirror array. Similar to the construction of large aperture telescopes [30], this optical system allows for the construction of a large, low f-number focusing mirror composed of multiple smaller, moderate f-number mirror segments. Here, each beamlet is incident on an individual segment of the parabolic mirror, whose piston and tip-tilt is controlled by three piezo actuators. By producing identical beamlets from a single aperture, the task of phasing multiple beams together is considerably simpler than combining multiple, separate amplifier beam lines.

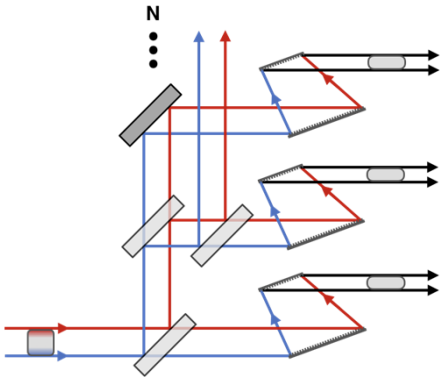

Fig. 4. Unit cell of a dispersion balanced beam splitter arrangement that can be repeated to split the beam into N identical copies. Each beamlet undergoes one transmission event in a beam splitter to ensure equal dispersion for each copy.

Optics EXPRESS

4. Analysis of pulse spatio-spectral and spatio-temporal structure

To determine the ideal spatio-spectral and spatio-temporal structure of the pulse that can be compressed by the six-grating compressor to a ~100 fs FTL pulse, we backpropagated the FTL pulse through the compressor and analyzed the beam-pulse structure at the input to the full six-grating compressor. This ray trace model was done with LightTrans' Virtual Lab Fusion [31]. In the ray tracing software an analysis plane records the spatio-spectral amplitude and phase of each frequency component in the pulse. With this we can create a 2D heat map of the pulse spatio-spectral structure to quantify the spatial chirp present in the beam, shown below in Fig. 5. Horizontal lineouts of the 2D map represent the spectral content at that transverse beam position (see Fig. 2 for the coordinate system). The asymmetry of the spectral content across the transverse beam center is a result of the diffracted angle of each beamlet, given by the grating diffraction equation, being nonlinear with respect to wavelength.

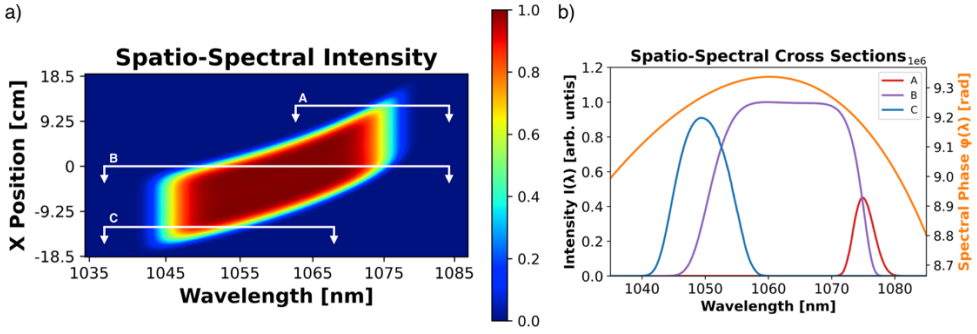

Fig. 5. The spectral cross-section of the beam changes with position along one of the beam's transverse axes (see Visualization 1). (a) 2D heatmap of the spatio-spectral pulse that is compressed by the six-grating compressor and (b) the spectral content and phase of the pulse at various beam transverse positions: 12.5 cm (A), 0 cm (B), and -12.5 cm (C).

Performing a line-by-line Fourier transform across the transverse beam width on the spectral pulse ascertains the full spatio-temporal pulse structure. Due to the high spectral frequency resolution needed for the large stretch factors involved, the Fourier transform was performed by a post-processing Python script [32]. A form of this hybrid ray tracing and numerical analysis technique was used by Laboratory for Laser Energetics to analyze the pulse structure from a tiled grating pulse compressor [33]. Below, in Fig. 6, the horizontal lineouts in the 2D spatio-temporal heat map give the pulse duration at each transverse cross-section of the beam. The spatial chirp results in a non-uniform pulse duration distribution along the spatial transverse axis of the beam. The maximum pulse duration FWHM is 18.9 ns at x-position 1.5 cm. The edges of the beam, while having a shorter pulse duration, have reduced energy content keeping the intensity low.

4.1. *Higher-order phase effects*

Clearly seen in Fig. 6(a) is an asymmetric temporal pulse structure that is due to the appreciable amount of third-order dispersion (TOD) removed by the compressor system; this is a natural consequence of any grating-based compressor. The substantial TOD reduces the effective pulse duration and can lead to increased B-integral accumulation in the amplification chain under full energy extraction conditions. This TOD effect should be minimized as much as possible to flatten the temporal cross-section and reduce the B-integral allowing for greater energy extraction from the amplifier.

The shortest possible FTL output pulse duration is desirable for building a high-peak-power laser. However, longer duration FTL output pulses may be useful for applications such as narrow

Optics EXPRESS

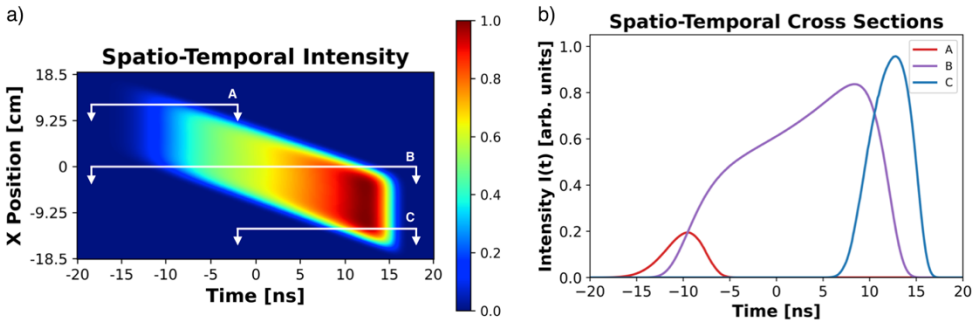

Fig. 6. Due to the changing spectral content along the one of the beam's transverse axis the temporal cross-section changes as well (see Visualization 2). (a) 2D heat map of the spatio-temporal structure of the pulse intensity that is compressed by the six-grating compressor and (b) the temporal cross-sections of the pulse at beam transverse positions 12.5 cm (A), 0 cm (B), and -12.5 cm (C) with FWHM pulse durations of 6.0 ns, 18.2 ns, and 4.6 ns respectively.

bandwidth laser-Compton scattering [34] and pumping OPCPA systems [10]. A longer FTL pulse duration equates to a smaller spectral bandwidth allowing for a larger grating separation for a fixed aperture grating pair. This modifies the spectral phase distribution that is removed by the compressor, which can be approximated as a Taylor series about the center frequency given by,

$$\varphi(\omega) \cong \varphi_0 + GD(\omega - \omega_0) + \frac{1}{2}GDD(\omega - \omega_0)^2 + \frac{1}{6}TOD(\omega - \omega_0)^3 + \cdots . \tag{4}$$

Here, φ_0 is the total phase of the center frequency, ω_0 is the center frequency, GD is the group delay, GDD is the group delay dispersion, and TOD is the third order dispersion. This phase function is fit to the spectral phase output from LightTrans to determine the GDD and TOD induced by the six-grating compressor. Table 2 details the maximum grating pair separation, the on-beam-center input pulse FWHM duration, as well as the GDD and TOD induced by the compressor configuration for various output FTL pulse durations.

Table 2. TFL pulse duration effects on six-grating compressor

		Grating Separation		Dispersion	
TFL Pulse FWHM [fs]	Stretched Pulse FWHM [ns]	G1/G2-G3/G4 [m]	G5/G6 [m]	GDD [fs^2]	TOD [fs^3]
100	18.2	1.914	0.780	-4.64E + 08	9.04E + 09
200	20.6	4.178	1.704	-1.01E + 09	2.03E + 10
500	21.1	10.684	4.356	-2.57E + 09	5.01E + 10
1000	20.7	21.365	8.715	-5.14E + 09	9.96E + 10

While the TOD term increases linearly with pulse duration, its effect on a spectral component's phase decreases to the third power with an increase in pulse duration due to the decreased spectral bandwidth. Figure 7, below, clearly shows this reduction of the TOD effect on the spatio-temporal intensity distribution as the pulse duration increases, which manifests itself as a temporal asymmetry.

An alternative route to modify the spatio-temporal distribution is to sculpt the spectral content of the pulse. Shown below in Fig. 8(b) is a modified spatio-temporal distribution resulting from a simple spectral sculpting, seen in Fig. 8(a). While the spectral sculpting has a precipitous effect on the spatio-temporal distribution, the effect on the FTL pulse duration and structure, plotted in

Optics EXPRESS

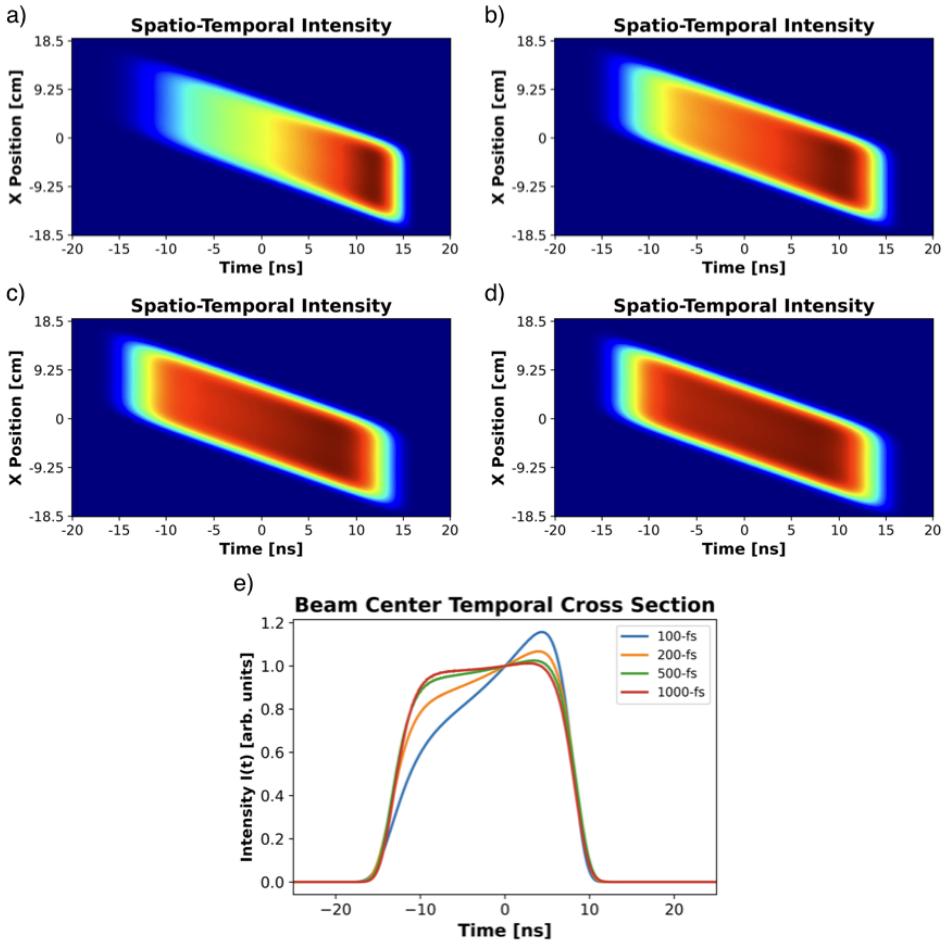

Fig. 7. Normalized spatio-temporal intensity distribution at the input of the six-grating compressor that compresses down to a FTL pulse with FWHM pulse duration of a) 100 fs, b) 200 fs, c) 500 fs, and d) 1000 fs. (e) Temporal cross section at the spatial center of the beam for the various TFL pulse widths.

Fig. 8(c) and (d), is minimal with the sculpted spectrum having a FTL FWHM of 100 fs. In this manner one can preserve the short duration FTL output pulse while removing any temporal spikes that would cause excessive B-integral accumulation in the amplifier. The sculpted spectrum in Fig. 8(a) is the full power spectrum of the pulse after it has been amplified and spatial chirp removed by the six-grating compressor. The input power spectrum to the amplifier is quite different due to typical gain saturation effects, where amplification is more efficient for the red wavelength components at the leading edge of the temporal pulse, as well as new transverse gain dynamics inherent to CPJBA. Here, both the spectrum and fluence vary with transverse position in the beam. The temporal gain saturation effects are well studied on NIF and are compensated for by appropriately shaping the spectrum prior to amplification in the front end injection laser system (ILS) [35]. The transverse gain effects are comparable to the transverse gain distribution experienced at NIF due to flash lamp pumping, where the center of the amplifier slab experiences higher gain than the edges [35]. For CPJBA, we can deal with this issue like NIF, by modulating

Optics EXPRESS

the transverse energy distribution in the laser front end [35], or by adjusting the gain distribution in the amplifier slab with a different spatial distribution of the pump energy.

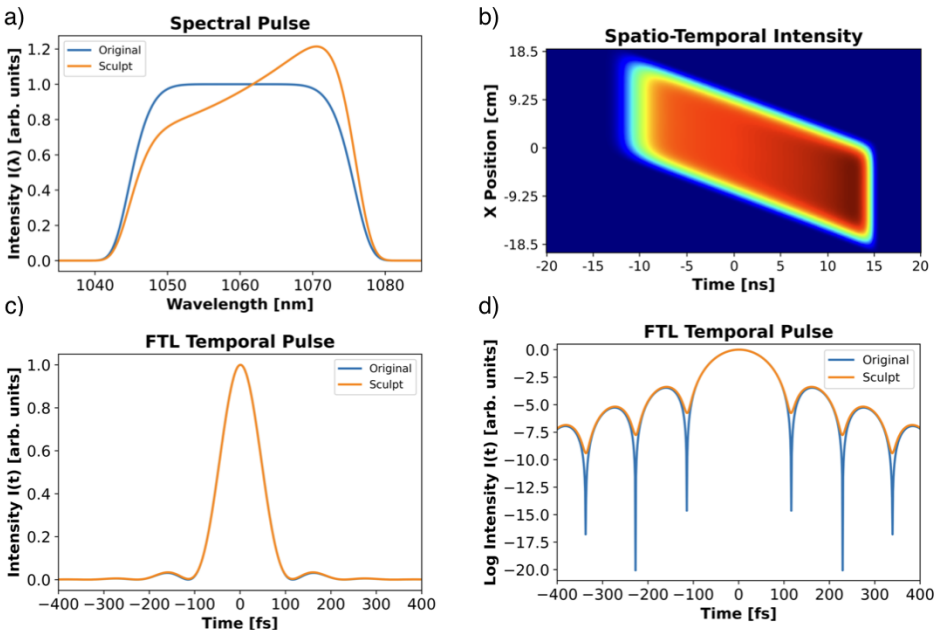

Fig. 8. (a) Spectrum of a sculpted pulse contrasted with the original non-sculpted spectrum. (b) The spatio-temporal profile of the sculpted pulse prior to entering the six-grating compressor. The resulting Fourier transform-limited temporal pulses of the sculpted and original spectrum (c) along with a log plot of the FTL temporal pulses (d).

5. Conclusion

With CPJBA one can increase the negative GDD produced by a fixed aperture grating pair by spatially chirping the beam in addition to temporally chirping. This chirped beam-pulse is recompressed, temporally and spatially, by a novel six-grating compressor arrangement that has been detailed here. Initial production of the chirped beam-pulse is possible by over stretching the pulse temporally with a multi-pass regenerative stretcher [36] and then spatially chirping the beam with a single pass grating pair. Early in the laser system the beam width is small and the modest spatial chirp required for CPJBA can be easily achieved with small aperture gratings and minor grating pair separation. Both the gain saturation and transverse gain effects of the chirped beam-pulse amplification will be pre-compensated in the front end of the laser system in a similar manner as the ILS on NIF. The full simulation of the amplifier and its optimization is planned for a future publication.

Using existing high-efficiency, high-groove-density grating designs and assuming the extension of multilayer dielectric grating manufacturing to 2 meter apertures, it is shown that CPJBA combined with the six-grating compressor can compress a spatially and temporally stretched 18.9 ns pulse to a spatially-uniform, FTL pulse duration of 100 fs. This stretched pulse duration has the potential to extract ~25 kJ from a large, single-aperture Nd:Mixed-Glass amplifier providing a promising pathway to extend high-peak-power laser systems into the exawatt-class without using tiled gratings or multiple independent amplifiers. A noticeable temporal pulse asymmetry on the stretched beam pulse is necessary in order to compensate for higher-order phase effects in the six-grating compressor. This asymmetry can be mitigated by either reducing the

Optics EXPRESS

spectral content of the desired FTL pulse or by sculpting the input pulse spectrum. While CPJBA was initially proposed with Nd:Mixed-Glass amplifiers in mind, this technique, along with the six-grating compressor, can be extended to many laser systems that require stretch-compression factors beyond what a traditional CPA arrangement can provide.

Disclosures. The authors declare no conflicts of interest.

Data availability. Data underlying the results presented in this paper are not publicly available at this time but may be obtained from the authors upon reasonable request.

References

1. M. W. L. Seggebruch, H. H. Effarah, E. Nelson, and C. P. J. Barty, "ICUIL World Map," The International Committee on Ultra-High Intensity Lasers (2020), https://www.icuil.org/activities/laser-labs.html
2. D. Strickland and G. Mourou, "Compression of amplified chirped optical pulses," Opt. Commun. **55**(6), 447–449 (1985).
3. W. Li, Z. Gan, L. Yu, C. Wang, Y. Liu, Z. Guo, L. Xu, M. Xu, Y. Hang, Y. Xu, J. Wang, P. Huang, H. Cao, B. Yao, X. Zhang, L. Chen, Y. Tang, S. Li, X. Liu, S. Li, M. He, D. Yin, X. Liang, Y. Leng, R. Li, and Z. Xu, "339 J high-energy Ti:sapphire chirped-pulse amplifier for 10 PW laser facility," Opt. Lett. **43**(22), 5681–5684 (2018).
4. G. A. Mourou, G. Korn, W. Sander, and J. L. Collier, "ELI – Extreme Light Infrastructure Whitebook: Science and Technology with Ultra-Intense Lasers," (THOSS Media GmbH, 2011).
5. T. Zhang, M. Yonemura, and Y. Kato, "An array-grating compressor for high-power chirped-pulse amplification lasers," Opt. Commun. **145**(1-6), 367–376 (1998).
6. J. Qiao, A. Kalb, M. J. Guardalben, G. King, D. Canning, and J. H. Kelly, "Large-aperture grating tiling by interferometry for petawatt chirped-pulse-amplification systems," Opt. Express **15**(15), 9562–9574 (2007).
7. G. R. Hays, E. W. Gaul, M. D. Martinez, and T. Ditmire, "Broad-spectrum neodymium-doped laser glasses for high-energy chirped-pulse amplification," Appl. Opt. **46**(21), 4813–4819 (2007).
8. N. Jourdain, U. Chaulagain, M. Havlik, D. Kramer, D. Kumar, I. Majerova, V. T. Tikhonchuk, G. Korn, and S. Weber, "The L4n laser beamline of the P3-installation: Towards high-repetition rate high-energy density physics at ELI-Beamlines," Matter Radiat. Extremes **6**(1), 015401 (2021).
9. B. M. Van Wonterghem, J. R. Murray, J. H. Campbell, D. R. Speck, C. E. Barker, I. C. Smith, D. F. Browning, and W. C. Behrendt, "National Ignition Facility commissioning and performance," Proc. of SPIE **5341**, 55–65 (2004).
10. Z. Li, K. Yoshiaki, and J. Kawanaka, "Simulating an ultra-broadband concept for Exawatt-class lasers," Sci. Rep. **11**(1), 151 (2021).
11. A. Cotel, M. Castaing, P. Pichon, and C. Le Blanc, "Phased-array grating compression for high-energy chirped pulse amplification lasers," Opt. Express **15**(5), 2742–2752 (2007).
12. C. P. J. Barty, "Optical chirped beam amplification and propagation," U.S. Patent 6804045 B2, (2004).
13. C. P. J. Barty, "The Nexawatt: A Strategy for Exawatt Peak Power Lasers Based on NIF and NIF-like Beam Lines," J. Phys.: Conf. Ser. **717**, 012086 (2016).
14. J. W. Yoon, Y. G. Kim, I. W. Choi, J. H. Sung, H. W. Lee, S. K. Lee, and C. H. Nam, "Realization of laser intensity over 10^{23} W/cm^2," Optica **8**(5), 630–635 (2021).
15. X. Zeng, K. Zhou, Y. Zuo, Q. Zhu, J. Su, X. Wang, X. Wang, X. Huang, X. Jiang, D. Jiang, Y. Guo, N. Xie, S. Zhou, Z. Wu, J. Mu, H. Peng, and F. Jing, "Multi-petawatt laser facility fully based on optical parametric chirped-pulse amplification," Opt. Lett. **42**(10), 2014–2017 (2017).
16. C. N. Danson, C. Haefner, J. Bromage, T. Butcher, J.-C. F. Chanteloup, E. A. Chowdhury, A. Galvanauskas, L. A. Gizzi, J. Hein, D. I. Hillier, N. W. Hopps, Y. Kato, E. A. Khazanov, R. Kodama, G. Korn, R. Li, Y. Li, J. Limpert, J. Ma, C. H. Nam, D. Neely, D. Papadopoulos, R. R. Penman, L. Qian, J. J. Rocca, A. A. Shaykin, C. W. Siders, C. Spindloe, S. Szatmari, R. M. G. M. Trines, J. Zhu, P. Zhu, and J. D. Zuegel, "Petawatt and exawatt class lasers worldwide," High Power Laser Sci. Eng. **7**(54), e54–55 (2019).
17. W. Koechner, *Solid-State Laser Engineering*, 6th ed. (Springer, 2006) Chap. 4.6.
18. C. C. Widmayer, J. M. Auerbach, R. B. Ehrlich, M. A. Henesian, J. T. Hunt, J. K. Lawson, D. Milam, P. A. Renard, D. R. Speck, P. J. Wegner, T. L. Weiland, W. H. Williams, C. R. Wolfe, and B. M. Van Wonterghem, "Producing National Ignition Facility (NIF)-Quality Beams on the Nova and Beamlet Lasers," Fusion Technol. **30**(3P2A), 464–470 (1996).
19. W. W. Simmons, J. T. Hunt, and W. E. Warren, "Light Propagation Through Large Laser Systems," IEEE J. Quantum Electron. **17**(9), 1727–1744 (1981).
20. C. P. J. Barty, M. Key, J. Britten, R. Beach, G. Beer, C. Brown, S. Bryan, J. Caird, T. Carlson, J. Crane, J. Dawson, A. C. Erlandson, D. Fittinghoff, M. Hermann, C. Hoaglan, A. Iyer, L. Jones II, I. Jovanovic, A. Komashko, O. Landen, Z. Liao, W. Molander, S. Mitchell, E. Moses, N. Nielsen, H. H. Nguyen, J. Nissen, S. Payne, D. Pennington, L. Risinger, M. Rushford, K. Skulina, M. Spaeth, B. Stuart, G. Tietbohl, and B. Wattellier, "An overview of LLNL high-energy short-pulse technology for advanced radiography of laser fusion experiments," Nucl. Fusion **44**(12), S266–S275 (2004).
21. L. J. Waxer, D. N. Maywar, J. H. Kelly, T. J. Kessler, B. E. Kruschwitz, S. J. Loucks, R. L. McCrory, D. D. Meyerhofer, S. F. B. Morse, C. Stoeckl, and J. D. Zuegel, "High-Energy Petawatt Capability for the Omega Laser," Optics & Photonics News **16**(7), 30–36 (2005).

Optics EXPRESS

22. J-L Miquel, C. Lion, and P. Vivini, "The Laser Mega-Joule: LMJ & PETAL status and Program Overview," J. Phys.: Conf. Ser. **688**, 012067 (2016).
23. J. Kawanaka, N. Miyanaga, H. Azechi, T. Kanabe, T. Jitsuno, K. Kondo, Y. Fujimoto, N. Morio, S. Matsuo, Y. Kawakami, R. Mizoguchi, K. Tauchi, M. Yano, S. Kudo, and Y. Ogura, "3.1-kJ Chirped-Pulse Power Amplification in the LFEX laser," J. Phys.: Conf. Ser. **112**(3), 032006 (2008).
24. E. B. Treacy, "Optical Pulse Compression with Diffraction Gratings," IEEE J. Quantum Electron. **5**(9), 454–458 (1969).
25. T. Erdogan and Plymouth Grating Laboratory, 5 Commerce Way, Carver, MA 02330, USA (personal communication, 2022).
26. W. H. Williams, J. K. Crane, D. A. Alessi, C. D. Boley, M. W. Bowers, A. D. Conder, J. G. Di Nicola, P. Di Nicola, C. Haefner, J. M Halpin, M. Y. Hamamoto, J. E. Heebner, M. R. Hermann, S. I. Herriot, D. C. Homoelle, D. H. Kalantar, T. E. Lanier, K. N. LaFortune, J. K. Lawson, R. R. Lowe-Webb, F. X. Morrissey, H. Nguyen, C. D. Orth, L. J. Pelz, M. A. Prantil, M. C. Rushford, R. A. Sacks, J. T Salmon, L. G. Seppala, M. J. Shaw, R. J. Sigurdsson, P. J. Wegner, C. C. Widmayer, S. T. Yang, and T. L. Zobrist, "Spatio-temporal focal spot characterization and modeling of the NIF ARC kilojoule picosecond laser," Appl. Opt. **60**(8), 2288–2303 (2021).
27. X. Gu, S. Akturk, and R. Trebino, "Spatial chirp in ultrafast optics," Opt. Commun. **242**(4-6), 599–604 (2004).
28. J. A. Britten, M. Molander, A. M. Komashko, and C. P. J. Barty, "Multilayer dielectric gratings for petawatt-class laser systems," Proc. SPIE **5273**, 1 (2004).
29. C. A. Haynam, P. J. Wegner, J. M. Auerbach, M. W. Bowers, S. N. Dixit, G. V. Erbert, G. M. Heestand, M. A. Henesian, M. R. Hermann, K. S. Jancaitis, K. R. Manes, C. D. Marshall, N. C. Mehta, J. Menapace, E. Moses, J. R. Murray, M. C. Nostrand, C. D. Orth, R. Patterson, R. A. Sacks, M. J. Shaw, M. Spaeth, S. B. Sutton, W. H. Williams, C. C. Widmayer, R. K. White, S. T. Yang, and B. M. Van Wonterghem, "National Ignition Facility laser performance status," Appl. Opt. **46**(16), 3276–3303 (2007).
30. I. Trumper, P. Hallibert, J. W. Arenberg, H. Kunieda, O. Guyon, H. P. Stahl, and D. W. Kim, "Optics technology for large-aperture space telescopes: from fabrication to final acceptance tests," Adv. Opt. Photon. **10**(3), 644–702 (2018).
31. LightTrans GmbH "Wyrowski VirtualLab Fusion: Technology Whitepapers," 2021, https://www.lighttrans.com/resources/downloads.html.
32. G. Van Rossum and F. L. Drake, "Python 3 Reference Manual," CreateSpace: Scotts Valley, CA; 2009.
33. B. Webb, M. J. Guardalben, C. Dorrer, S. Bucht, and J. Bromage, "Simulation of grating compressor misalignment tolerances and mitigation strategies for chirped-pulse-amplification systems of varying bandwidths and beam sizes," Appl. Opt. **58**(2), 234–243 (2019).
34. C. P. J. Barty, "Method for efficient, narrow-bandwidth, laser Compton x-ray and gamma-ray sources," U.S. Patent 9706631 (2017).
35. M. L. Spaeth, K. R. Manes, D. H. Kalantar, P. E. Miller, J. E. Heebner, E. S. Bliss, D. R. Speck, T. G. Parham, P. K. Whitman, P. J. Wegner, P. A. Baisden, J. A. Menapace, M. W. Bowers, S. J. Cohen, T. I. Suratwala, J. M. Di Nicola, M. A. Newton, J. J. Adams, J. B. Trenholme, R. G. Finucane, R. E. Bonanno, D. C. Rardin, P. A. Arnold, S. N. Dixit, G. V. Erbert, A. C. Erlandson, J. E. Fair, E. Feigenbaun, W. H. Gourdin, R. A. Hawley, J. Honig, R. K. House, K. S. Jancaitis, K. N. LaFortune, D. W. Larson, B. J. Le Galloudec, J. D. Lindl, B. J. MacGowan, C. D. Marshall, K. P. McCandless, R. W. McCraken, R. C. Montesanti, E. I Moses, M. C. Nostrand, J. A. Pryatel, V. S. Roberts, S. B. Rodriguez, A. W. Rowe, R. A. Sacks, J. T. Salmon, M. J. Shaw, S. Sommer, C. J. Stolz, G. L. Tietbohl, C. C. Widmayer, and R. Zacharias, "Description of the NIF Laser," Fusion Sci. Technol. **69**(1), 25–145 (2016).
36. H. Su, Y. Peng, Y. Li, X. Lu, J. Chen, P. Wang, X. Lv, B. Shao, and Y. Leng, "Multipass active stretcher with large chirp for high-flux ultra-intense lasers," Opt. Lett. **44**(8), 1980–1983 (2019).